Sensors **2015**, *15*, 17693-17714; doi:10.3390/s150717693

OPEN ACCESS
sensors
ISSN 1424-8220
www.mdpi.com/journal/sensors

Article

Fast T Wave Detection Calibrated by Clinical Knowledge with Annotation of P and T Waves

Mohamed Elgendi [1,2,*], Bjoern Eskofier [3] and Derek Abbott [4]

[1] Electrical and Computer Engineering in Medicine Group, University of British Columbia and BC Children's Hospital, Vancouver, BC V6H 3N1, Canada
[2] Department of Computing Science, University of Alberta, Edmonton, AB T6G 2E8, Canada
[3] Pattern Recognition Lab, Friedrich-Alexander University Erlangen-Nuernbeg, Haberstr. 2, 91058 Erlangen, Germany; E-Mail: eskofier@cs.fau.de
[4] School of Electrical and Electronic Engineering, University of Adelaide, Adelaide SA 5005, Australia; E-Mail: derek.abbott@adelaide.edu.au

* Author to whom correspondence should be addressed; E-Mail: moe.elgendi@gmail.com; Tel.: +1-604-600-4139.

Academic Editor: Vittorio M.N. Passaro

Received: 1 June 2015 / Accepted: 10 July 2015 / Published: 21 July 2015

Abstract: Background: There are limited studies on the automatic detection of T waves in arrhythmic electrocardiogram (ECG) signals. This is perhaps because there is no available arrhythmia dataset with annotated T waves. There is a growing need to develop numerically-efficient algorithms that can accommodate the new trend of battery-driven ECG devices. Moreover, there is also a need to analyze long-term recorded signals in a reliable and time-efficient manner, therefore improving the diagnostic ability of mobile devices and point-of-care technologies. Methods: Here, the T wave annotation of the well-known MIT-BIH arrhythmia database is discussed and provided. Moreover, a simple fast method for detecting T waves is introduced. A typical T wave detection method has been reduced to a basic approach consisting of two moving averages and dynamic thresholds. The dynamic thresholds were calibrated using four clinically known types of sinus node response to atrial premature depolarization (compensation, reset, interpolation, and reentry). Results: The determination of T wave peaks is performed and the proposed algorithm is evaluated on two well-known databases, the QT and MIT-BIH Arrhythmia databases. The detector obtained a sensitivity of 97.14% and a positive predictivity of 99.29% over the first lead of the validation databases (total of 221,186 beats). Conclusions: We present a simple yet

very reliable T wave detection algorithm that can be potentially implemented on mobile battery-driven devices. In contrast to complex methods, it can be easily implemented in a digital filter design.

Keywords: arrhythmia; affordable healthcare; moving averages

1. Introduction

According to the World Health Organization, cardiovascular diseases (CVDs) are the number one cause of death globally; more people die annually from CVDs than from any other cause [1]. An estimated 17.3 million people died from CVDs in 2008, representing 30% of all global deaths [1]. Of these deaths, an estimated 7.3 million were due to coronary heart disease and 6.2 million were due to stroke [1]. Thus, medical researchers have placed significant importance on cardiac health research. This has led to a strong focus on technological advances with respect to cardiac function assessment. One such research pathway is the improvement of conventional cardiovascular diagnosis technologies used in hospitals and clinics.

The most common clinical cardiac test is electrocardiogram (ECG) analysis as it is simple, risk-free, and inexpensive [2]. The signal of each heart beat contains five main waves: the P, Q, R, S, and T waves. The automatic detection of these waves is critical for reliable cardiovascular assessment, such as diagnosing cardiac arrhythmias [3–6], understanding autonomic regulation of the cardiovascular system during sleep and hypertension [7,8], detecting breathing disorders such as obstructive sleep apnea syndrome [9,10], and monitoring other structural or functional cardiac disorders.

The detection of R peaks and QRS complexes has been extensively investigated over the past two decades [11]. Conversely, T wave detection has not been investigated as widely as QRS detection, and the T wave detection problem is still far from being solved [12–15]. Reliable T wave detection is more challenging than QRS complex detection for several reasons, including low amplitudes, low signal-to-noise ratio (SNR), amplitude and morphology variability, and possible overlapping of the P wave and T wave [11,16]. Nevertheless, accurate T wave detection is mandatory for a variety of (differential) diagnostic tasks, such as acute coronary syndrome [17], acute myocardial infarction [18], or potentially fatal arrhythmias [19]. To our knowledge, there was no attempt to develop an ECG detector based on existing clinical knowledge. Thus, in this paper, we investigated the possibility of applying clinical knowledge to build a T wave detection algorithm.

In addition, in the near future, it is expected that Holter devices, which are traditionally used for ECG analysis in the clinic, will be replaced by portable battery-operated devices, such as mobile phones [11]. Therefore, there is a need for a simple, fast, and computationally efficient algorithm to detect arrhythmias efficiently in real time. To develop fast robust algorithms for detecting Arrhythmia in ECG collected by portable, wearable, and battery-driven devices, first we require fully annotated arrhythmia ECG signals as a benchmark for evaluation. Unfortunately, the MIT-BIH Arrhythmia database [20] includes *only* the annotations of R peaks. Therefore, in this study, we annotated T waves in the MIT-BIH Arrhythmia

database [20,21]. Moreover, a new fast robust algorithm consisting of two moving averages that are calibrated by a clinical knowledge base is presented.

2. Materials and Methods

2.1. Data Used

Several standard ECG databases are available for the evaluation of QRS detection algorithms for ECG signals. Most of these databases contain annotated files for R peaks but not for T waves. To demonstrate the applicability of the algorithm presented in this paper, two databases are used in this study: one self-annotated database and one standard annotated database.

2.1.1. Database Annotated Under This Study

An expert manually annotated the P and T peaks of the MIT-BIH Arrhythmia database [20,21] to be used in evaluation for the following reasons:

1. The MIT-BIH database contains 30-min recordings for each patient, which is considerably longer than the records in many other databases, such as the Common Standards for Electrocardiography database, which contains 10-s recordings [22].
2. The MIT-BIH Arrhythmia database contains records of normal ECG signals and records of ECG signals that are affected by non-stationary effects, low SNR, premature atrial complexes, premature ventricular complexes, left bundle blocks, and right bundle blocks. This provides an opportunity to test the robustness of T wave detection methods.
3. The database contains 23 records (the "100 series") that were chosen at random from a set of more than 4000 24-h Holter tapes, and 25 records (the "200 series") that were selected from the same set, including a variety of rare and clinically important ECG segments [20]. Several records in the 200 series have abnormal rhythms and QRS morphologies and they suffer from a low SNR. These issues are expected to present significant difficulties for any ECG signal analysis algorithm [20].

Figures 1–3 demonstrate examples for annotation of T waves for different beats in the MIT-BIH Arrhythmia database. There was no automated aid provided during the annotation process and only channel one (Lead I) was annotated. For special cases, such as biphasic T waves, the middle point of the wave was considered as a T wave. The annotation file of P and T waves can be downloaded from [23].

2.1.2. Standard Annotated Database

As the MIT-BIH database is self-annotated, the validation of the detector must be carried out using a standard annotated database. For this purpose, the easily-available QT database [24] is used. This database was annotated by two cardiologists and includes different morphologies such as ST change, supraventricular arrhythmia, normal sinus rhythm, sudden death, and long-term ECG signals. The two cardiologists annotated only selected beats (3542 beats in a file called ".q1c") in all recordings except two recordings: "sel35" and "sel37". However, the automatic annotation of the whole database was carried using *ecgpuwave* software, which is saved in the ".pu" file. In this work, the T peaks of Lead I of the whole QT database are used for validation as they are more salient and certain compared to

the onset and offset. In this work, the T peaks of the whole QT database are used for validation as they are more salient and certain compared to the onset and offset. Moreover, once the T peak is detected correctly, searching for the onset and offset is a relatively easy step; however, this is not the focus of this study.

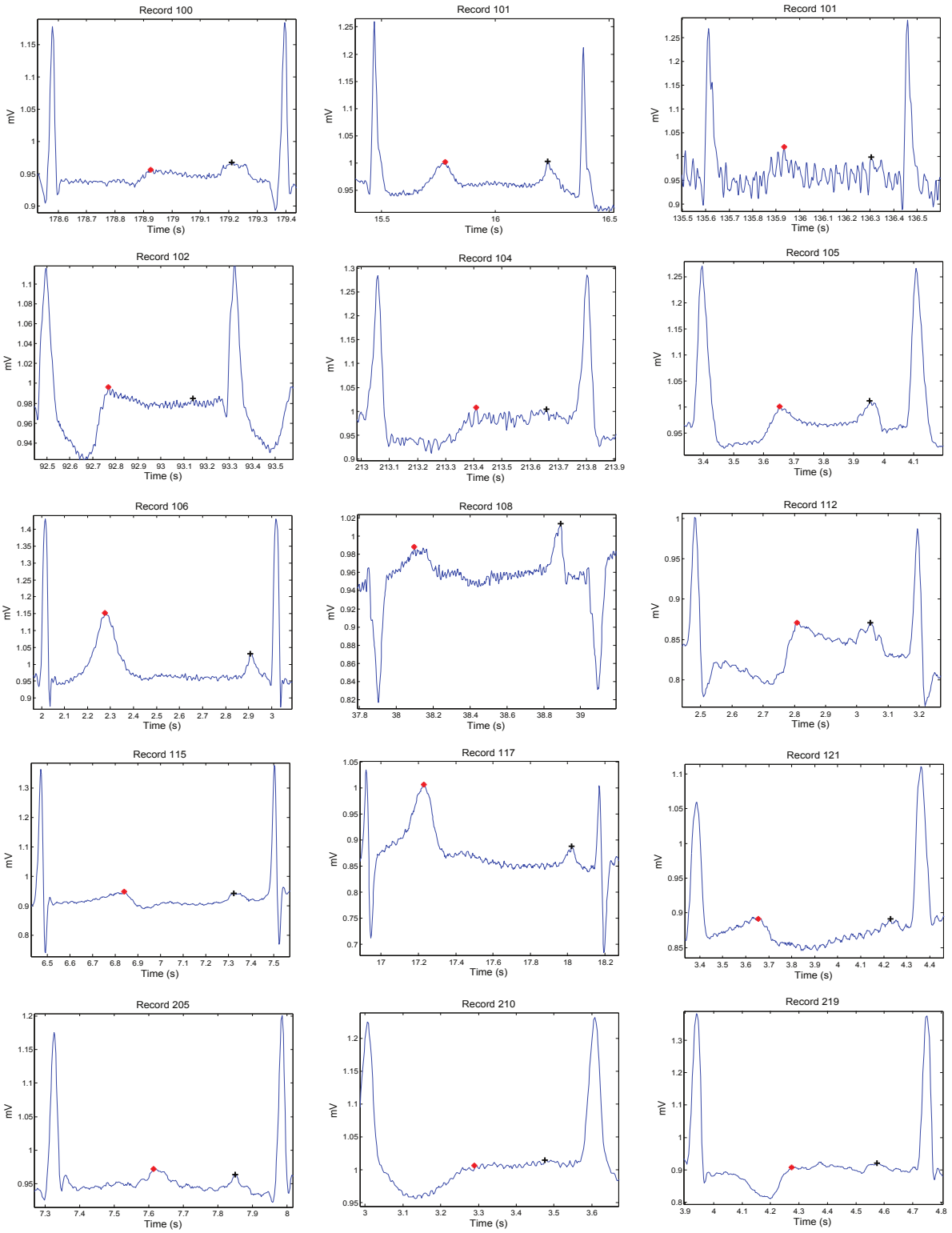

Figure 1. Annotation of P and T waves in normal beats. Here, "+" represents the P wave and "*" represents the T wave. Note that the higher peaks represent the QRS complex.

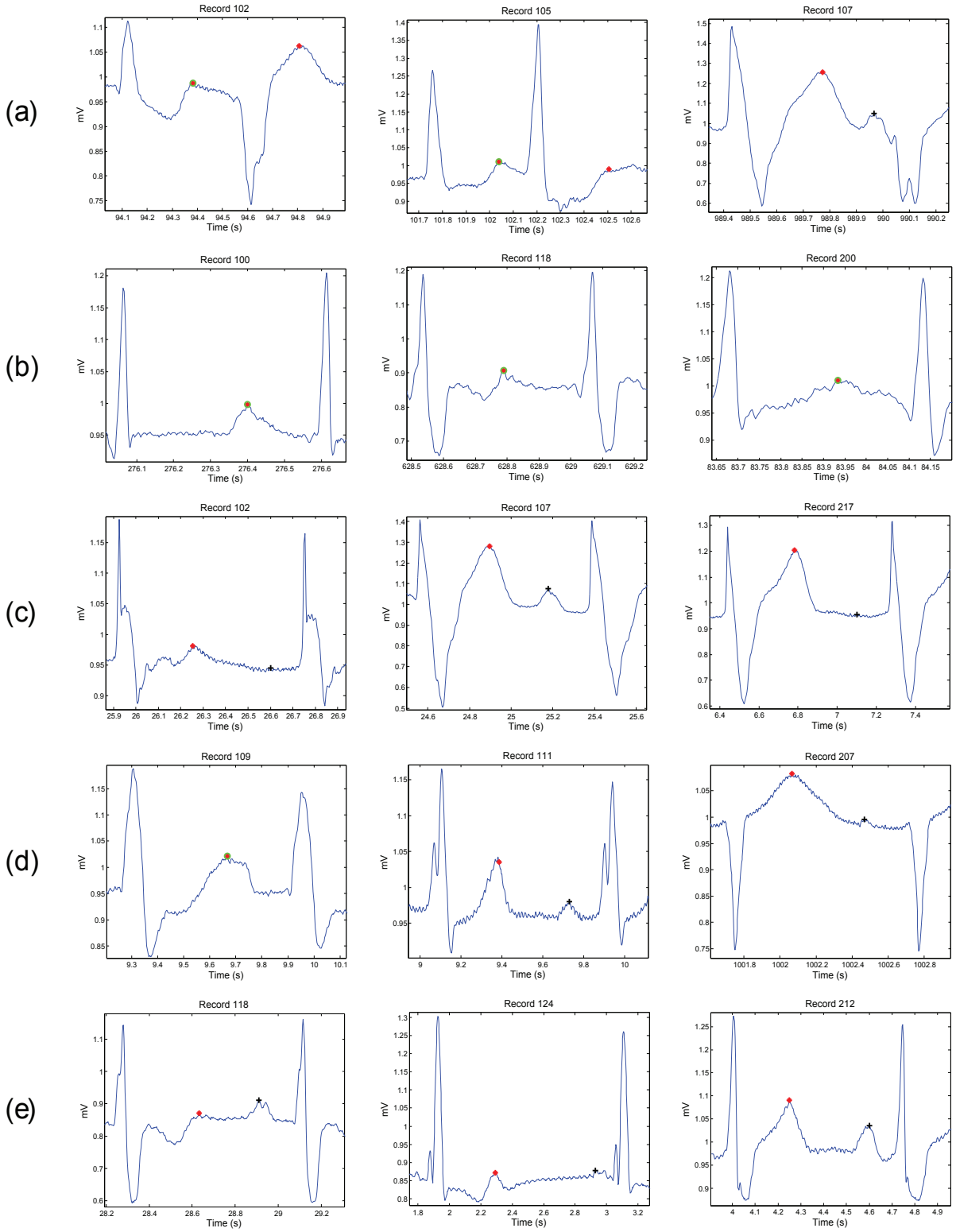

Figure 2. Annotation of Pand T waves in irregular heart beats. Each row contains three different morphologies for a certain type of arrhythmia: (**a**) premature ventricular beats; (**b**) premature atrial beats; (**c**) paced beats; (**d**) left bundle branch block beats; (**e**) right bundle branch block beats. Here, "+" represents the P wave and "*" represents the T wave, while the green circle with asterisk represents merged P and T waves.

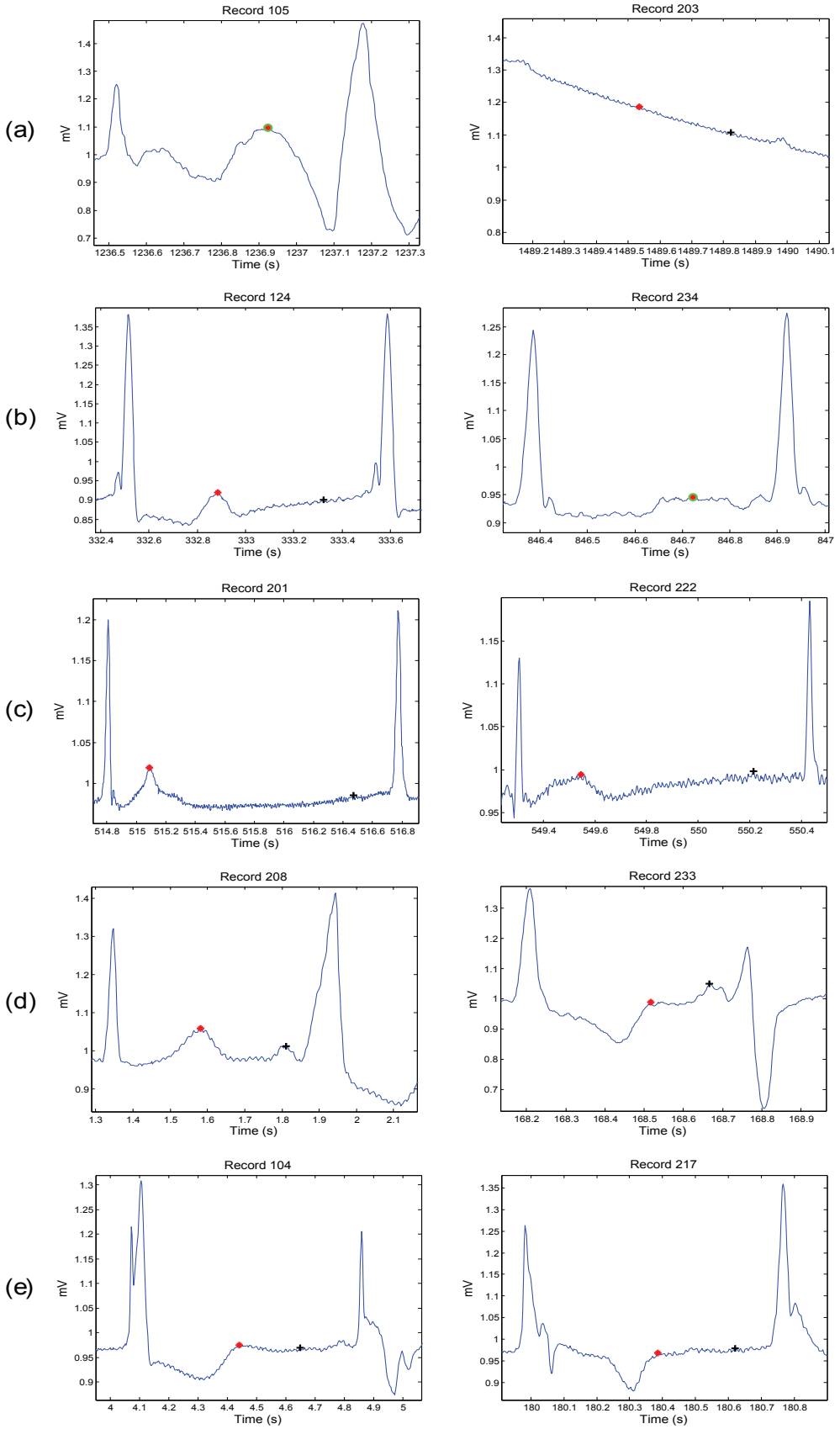

Figure 3. Annotation of P and T waves in unusual beats. Each row contains two different morphologies for a certain type of unusual beats: (**a**) unclassified beats; (**b**) nodal premature beat; (**c**) nodal escape beat; (**d**) fusion of ventricular and normal beat; (**e**) fusion of paced and normal beat. Here, "+" represents the P wave and "*" represents the T wave, while the green circle with asterisk represents merged P and T waves.

2.2. T Wave Detection Algorithm

In this study, a fast robust knowledge-based T wave detection algorithm is discussed and evaluated. The algorithm is based on the framework proposed by Elgendi for detecting QRS complexes in ECG signals [25,26], for detecting systolic waves in photoplethysmogram signals [27], detecting a waves [28], and detecting c, d, e waves [29] in acceleration photoplethysmogram (PPG) signals. We build upon this approach to detect T waves. The method consists of three main stages: pre-processing (clinical knowledge, bandpass filtering, squaring, and QRS removal), feature extraction (generating potential blocks using two moving averages), and classification (thresholding). The structure of the algorithm is given in Figure 4.

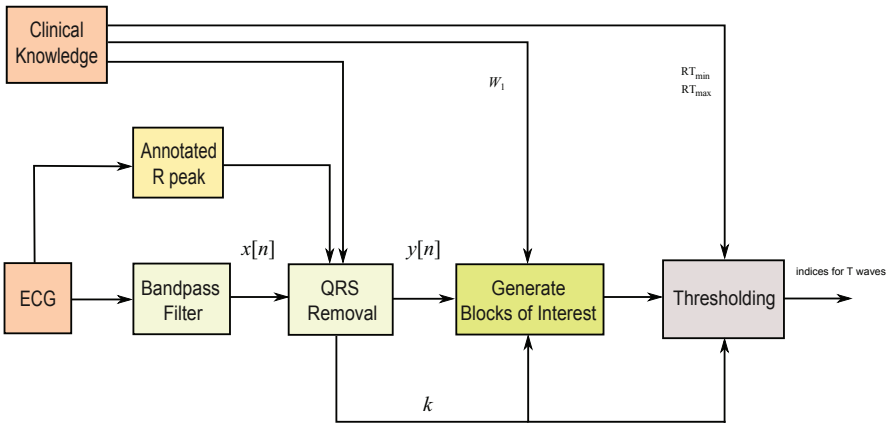

Figure 4. Structure of the T waves detection algorithm. The algorithm consists of three main stages: pre-processing (clinical knowledge, bandpass filtering, squaring, and QRS removal), feature extraction (generating potential blocks using two moving averages), and classification (thresholding).

2.2.1. Bandpass Filter

Most of the energy of T waves lies below 10 Hz [30,31]; thus, a zero-phase second-order Butterworth filter, with a 0.5–10 Hz bandpass, is implemented to remove the baseline wander and high frequencies that do not contribute to the T waves. The output of the zero-phase Butterworth filter applied to the ECG signal produces a filtered signal $x[n]$.

2.2.2. QRS Removal

The QRS removal step based on the relative distance of the T wave to its associated R peak. Removing the QRS complex has two advantages: (1) T waves become the dominant feature in the processed signal; and (2) it simplifies the search for T waves relative to the position of R peaks. In this study, as proof of concept, the R peaks provided in the MIT-BIH Arrhythmia and QT databases are used. Removing the QRS complex is performed by setting the signal to zero for the duration of the QRS complex.

The limits (thresholds) of the RT distance are determined using ECG clinical knowledge. The signal $y[n]$ is initialized as equal to the filtered ECG $x[n]$ signal. The QRS removal length thresholds are determined based on the clinical phases of the RR intervals. As the duration of the QRS complex varies

with the heart beat type, a clinical database is required to remove the QRS complex, according to its type. Roskamm and Csapo divided the ECG into four phases: compensation, reset, interpolation, and reentry [32]. Based on their analysis, in the compensation phase (Figure 5a), the second beat (850 ms) is followed by a prolonged beat (1150 ms) to compensate the two beats duration (2000 ms). During the reset phase (Figure 5b), the second beat (650 ms) is followed by a prolonged beat (1150 ms), while in the interpolation (Figure 5c), the second beat (400 ms) is followed by an irregular beat (600 ms). Finally, in the reentry phase (Figure 5d), the second beat (300 ms) is followed by a rapid irregular beat (400 ms); however, an extra category is added to capture complex arrhythmias (repetitive, bigeminy, or trigeminy). The output of this stage will produce an updated $y[n]$ signal.

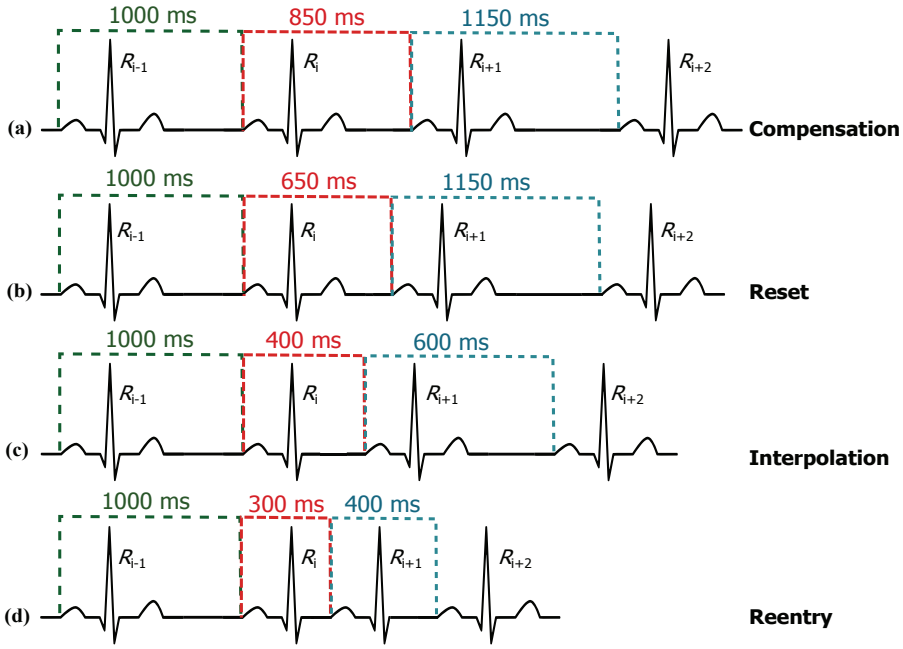

Figure 5. Types of sinus node response to atrial premature depolarization (adapted from [32]).

Based on the clinical information presented in Figure 5, the ratio of the second beat duration to the first and third beat duration generates a rule-based knowledge representation, as shown in Figure 6. For example, in the case of reentry (left branch of the flowchart in Figure 6), the first threshold is calculated by dividing the duration between the third and the fourth beat ($R_{i+2} - R_{i+1} = 400$ ms) by the duration between the two and the third beat ($R_{i+1} - R_i = 300$ ms) resulting as 1.33; however, this value was calculated with reference to the duration between first beat and second beat ($R_i - R_{i-1} = 1000$ ms)—this generates the first rule: $\mathrm{RR2} \leq 1.33\ \mathrm{RR1}$, where $\mathrm{RR1} = R_i - R_{i-1}$, $\mathrm{RR2} = R_{i+1} - R_i$, and i is the beat index. The second threshold is the expected total duration of the second and third beats (300 ms + 400 ms), which equals 0.7 s—this generates the second rule: $(\mathrm{RR1} + \mathrm{RR2}) \leq 0.7 f_s$. On the right side the flowchart in Figure 6, in the case of reentry, the first threshold is calculated by dividing the duration between the third and the fourth beat ($R_{i+1} - R_i = 300$ ms) by the duration between the first and the second beat ($R_i - R_{i-1} = 1000$ ms) resulting as 0.3—this generates the first rule: $\mathrm{RR2} \leq 0.3\ \mathrm{RR1}$, while the second threshold is based on the duration between the first and the second beat ($R_i - R_{i-1} = 1000$ ms) which is 1 s (or f_s)—this generates the second rule: $\mathrm{RR1} \leq f_s$. Similarly, all other rules were created for the other four ECG phases.

Figure 6. Rule-based knowledge representation of QRS removal based on the clinical knowledge shown in Figure 5.

During the QRS removal, the RR interval that satisfied each category is saved and referred to as RR_k, where k is the category type (compensation, reset, interpolation, reentry, and complex arrhythmias). The normalized RR intervals average in each category is calculated as $M_c = (\sum_{j=1}^{l} \mathrm{RR}_{c,j})/(lf_s)$, where l is the number of RR intervals saved in category c, and f_s is the sampling frequency. Dividing M_c by f_s is sufficient as it is equivalent to the average RR interval in healthy subjects.

2.2.3. Generating Blocks of Interest

Blocks of interest are generated using two event-related moving averages that demarcate the areas of T waves, a method which was first introduced in [33]. The particular method used to generate blocks of interest has been mathematically shown to detect a waves [28], QRS complexes [25], and systolic waves in PPG signals [27]. In this procedure, the first moving average ($\mathrm{MA}_{\mathrm{peak}}$) is used to emphasize the peak of the T wave area, as the dotted signal shown in Figure 7, and is given by

$$\mathrm{MA}_{\mathrm{peak}}[n] = \frac{1}{W_1}(y[n-(W_1-1)/2] + \cdots + y[n] + \cdots + y[n+(W_1-1)/2]) \quad (1)$$

where W_1 represents the window size of approximately the peak duration of the T wave in ECG signals. The initial value for W_1 of 70 ms is determined by Trahanias [34]. However, as the ECG signals may contain different arrhythmias the value of W_1 will be calculated relative to the most frequent RR intervals in all five categories ($k = \max_c M_c$). Then, the value of $W_1 = (70\ \mathrm{ms} \times f_s) \times k$, and the result is rounded to the nearest odd integer. The second moving average ($\mathrm{MA}_{\mathrm{Twave}}$) is used to emphasize the T wave area to be used as a threshold for the first moving average, shown as a dashed signal Figure 7, and is given by

$$\mathrm{MA}_{\mathrm{Twave}}[n] = \frac{1}{W_2}(y[n-(W_2-1)/2] + \cdots + y[n] + \cdots + y[n+(W_2-1)/2]) \quad (2)$$

where W_2 represents the window size of approximately the T wave duration. The initial value for W_2 of 140 ms is determined by Laguna *et al.* [35]. However, as the ECG signals may contain different arrhythmias, the value of W_2 will be calculated relative to the most frequent RR intervals in all five categories (k). Then, the value of $W_2 = (140\ \mathrm{ms} \times f_s) \times k$, and the result is rounded to the nearest odd integer. For example, the total values of W_1 and W_2 for detecting T waves in record 100 from MIT-BIH Arrhythmia database were 20 samples (55.6 ms) and 40 samples (111.2 ms); respectively.

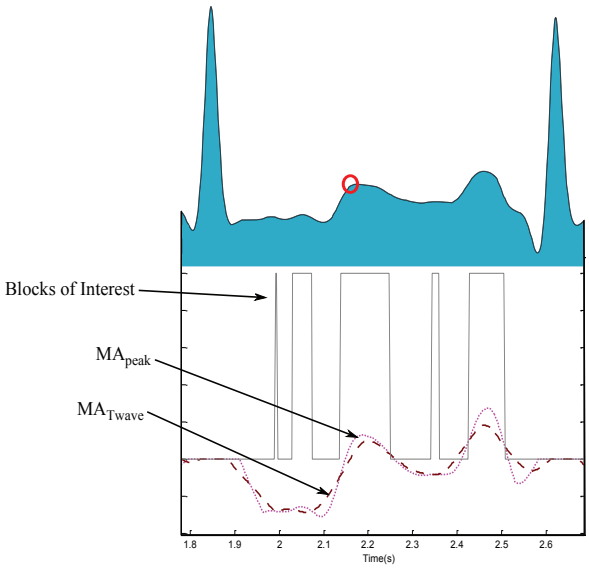

Figure 7. Demonstrating the effectiveness of using two moving averages to detect T waves. The dotted line is the first moving average, while the dashed line is the second moving average. The red circle is the detected T wave peak.

2.2.4. Thresholding

In this stage, the blocks of interest are generated by comparing the $\mathrm{MA}_{\mathrm{peak}}$ signal with $\mathrm{MA}_{\mathrm{Twave}}$. Many blocks of interest will be generated, some of which will contain the T wave and others will contain P waves, U waves, and noise. Therefore, the next step is to reject blocks that result from noise. Rejection is based on the relative positions of P and T waves to R peaks and anticipated peak width.

To determine whether the detected blocks contain T waves or not, the number of blocks in each consecutive RR interval is counted. A threshold based on the distance of the maximum point within a

block to the R peak is applied to distinguish P waves from T waves and noise, as shown in Figure 8. The search regions for T waves in terms of time occurrence with respect to the current R peak (R_i) and the next R peak (R_{i+1}) are calculated as

$$\mathrm{R}_i\mathrm{T}_{\min} = \mathrm{D}_{\min}\mathrm{R}_i\mathrm{R}_{i+1} \tag{3}$$

$$\mathrm{R}_i\mathrm{T}_{\max} = \mathrm{D}_{\max}\mathrm{R}_i\mathrm{R}_{i+1} \tag{4}$$

where $\mathrm{R}_i\mathrm{T}_{\min}$ represents the minimum dynamic interval between the T wave and the current R peak, $\mathrm{R}_i\mathrm{T}_{\max}$ represents the maximum dynamic interval between the T wave and the current R peak, while $\mathrm{R}_i\mathrm{R}_{i+1}$ represents the interval between R_i and R_{i+1}. The exact values for $\mathrm{D}_{\min}$ and $\mathrm{D}_{\max}$ are 170 ms and 800 ms, respectively, as determined by Schimpf *et al.* [36] to represent the minimum RT durations for subjects with arrhythmia and maximum RT duration for healthy subjects. All detected blocks go through a durational threshold to reject the undesired blocks called THR_1, which rejects the blocks that contain P wave, U wave, and noise. By applying the THR_1 threshold, the accepted blocks will contain T peaks only,

$$\mathrm{THR}_1 = W_1 \tag{5}$$

After applying the relative-position thresholds, there are three possibilities for the number of detected blocks within the area of interest:

1. **Zero:** if there is no block detected, it means the algorithm failed to detect a T wave in the current RR interval.
2. **One:** if there is one detected block, it means the algorithm succeeds in detecting T wave, P and T waves are most likely merged within one block, which is marked as a circle with a black asterisk inside (see Figure 9i,j).
3. **More than one:** if there are multiple detected blocks, as shown in Figure 7, it means one of the detected blocks contains T waves. However, in this work the nearest block to the current R peak is considered a T wave.

The last stage is to find the maximum absolute value within each block to detect the peak of T wave. The detected T wave peaks are compared to the annotated T wave peaks to determine whether they were detected correctly. The search range for the true T wave peak is fixed to $\pm$30 ms for both databases, to ensure consistency of comparison. The search region of 30 ms is good enough for diagnostics as it is less than W_1.

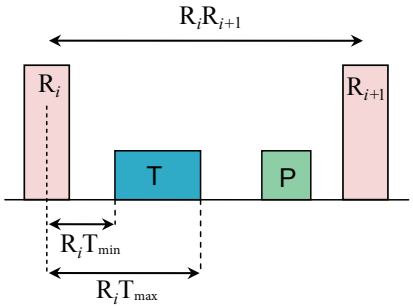

Figure 8. Search regions for T waves in terms of time occurrence with respect to the current R peak (R_i) and the next R peak (R_{i+1}). Where $\mathrm{R}_i\mathrm{T}_{\min}$ represents the minimum interval between the T wave and current R peak and $\mathrm{R}_i\mathrm{T}_{\max}$ represents the maximum interval between the T wave and the current R peak.

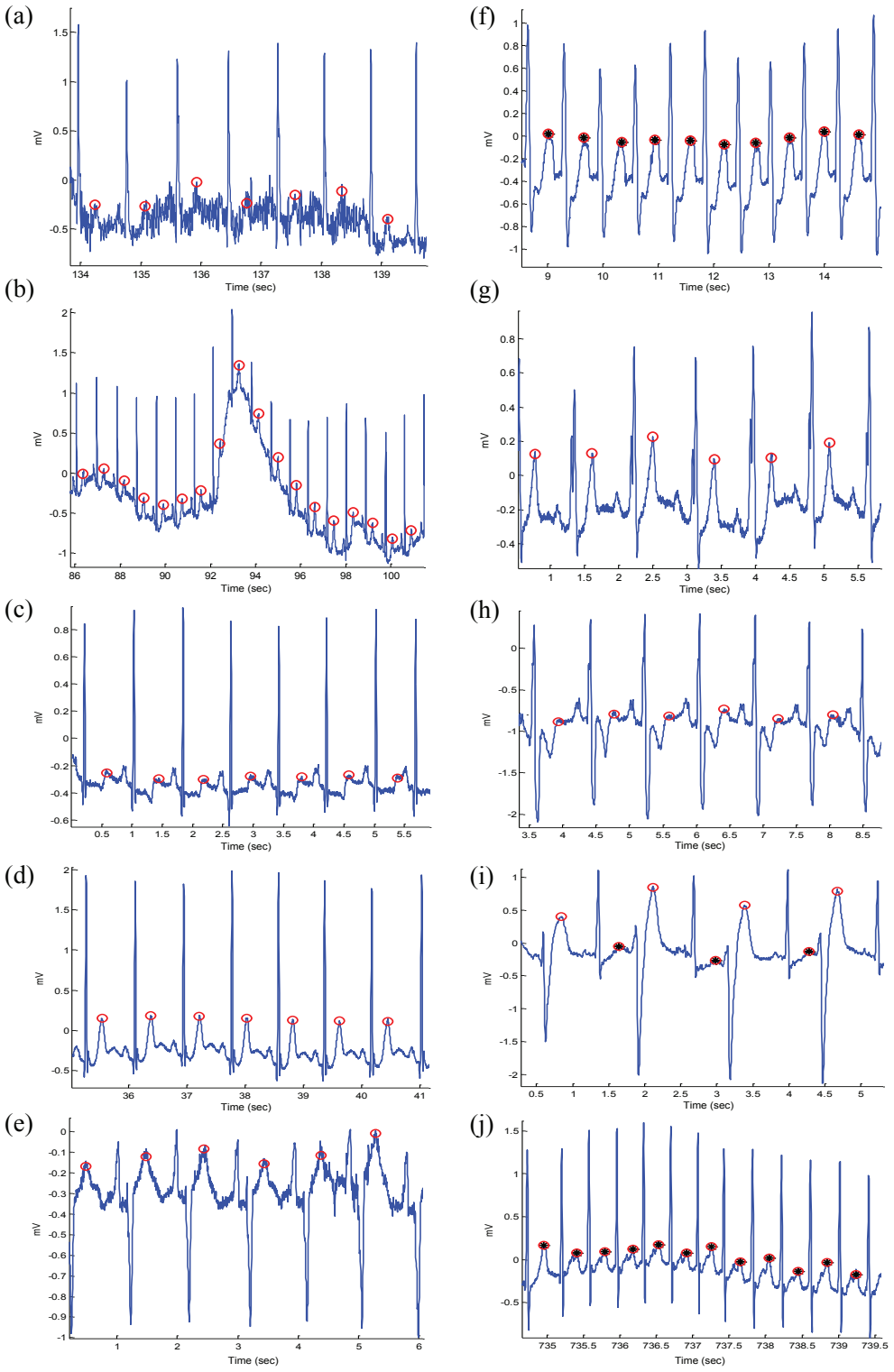

Figure 9. Demonstrating the performance of the proposed T wave detection algorithm on the MIT-BIH Arrhythmia database. The algorithm succeeds to detect T wave peaks in electrocardiogram (ECG) signals that contain: (**a**) high-frequency noise; (**b**) baseline wander; (**c**) normal sinus rhythm without U waves; (**d**) normal sinus rhythm with U waves; (**e**) normal sinus rhythm with negative polarization; (**f**) left bundle branch block (LBBB) beats with merged P and T waves; (**g**) LBBB beats; (**h**) right bundle branch block (RBBB) beats from record 118; (**i**) premature ventricular contraction (PVC) beats from record 200; (**j**) premature atrial contraction (PAC) beats from record 209. Here, the empty red circle represents the detected T wave while the a circle with a black asterisk represents detection of merged P and T waves.

3. Results

The algorithm was evaluated using the MIT-BIH database. The T waves were detected successfully even when the P and T waves are merged in Arrhythmia ECG signals that are affected by: high-frequency noise, baseline wander, normal sinus rhythm (NSR), left bundle branch block (LBBB), right bundle branch block (RBBB), premature ventricular contraction (PVC), and premature atrial contraction (PAC). All of the reasons for detection failure are described below. High-frequency noise results from the instrumentation amplifiers, recording system, and ambient electromagnetic signals received by the cables. The signal shown in Figure 9a has been corrupted by power-line interference at 60 Hz and its harmonics and other high frequencies. It can be seen that the proposed algorithm is robust to noise. Moreover, the proposed algorithm is not sensitive to baseline wander and detected the T waves correctly, as shown in Figure 9b. This is because the moving averages were applied to the bandpass filtered ECG signal—which is discussed in the Bandpass Filter Subsection.

The NSR is a normal ECG cycle; it is initiated by the sinoatrial node and consists of a P wave followed, after a brief pause, by a QRS complex and then a T wave [37]. The proposed algorithm correctly detected T waves in three types of normal beats: (1) NSR without U waves (record 100 of the MIT-BIH database), as shown in Figure 9c; (2) NSR with U waves (record 103), as shown Figure 9d; and (3) NSR with negative polarization (record 108), as shown Figure 9e. The LBBB results from conduction delays or blocks at any site in the intraventricular conduction system, including the main LBBB and the bundle of His. The result of an LBBB is an extensive reorganization of the activation pattern of the left ventricles [37]. The proposed algorithms successfully detected normal and merged P and T waves in two types of LBBBs: (1) LBBB beats with merged P and T waves (record 109), as shown in Figure 9f and (2) LBBB beats with normal T waves (record 111), as shown in Figure 9g. However, RBBB is a result of a conduction delay in a portion of the right-sided intra-ventricular conduction system. The delay can occur in the main RBBB itself, in the bundle of His, or in the distal right ventricular conduction system. The RBBBs may be caused by a minor trauma, such as right ventricular catheterization [37]. As shown in Figure 9h, the proposed algorithms succeeded in detecting the T waves in ECG signals of RBBB (record 118).

The PVCs are characterized by the premature occurrence of a QRS complex that is abnormal in shape, and that has a longer duration than normal QRS complexes, generally exceeding 120 ms [37]. The T wave is commonly large and opposite in direction to the major deflection of the QRS. In general, the QRS complex is not preceded by a P wave, but it can be preceded by a non-conducted sinus P wave occurring at the expected time [37]. In Figure 9i, a special case of PVC is shown, called bigeminy, where the premature ventricular beats occur after every normal beat in an alternating pattern.

The proposed algorithm succeeded in detecting the T waves in the normal beats and the T waves in the premature ventricular beats (record 200). Note that PACs are among the most common causes of irregular pulses and can originate from any area in the heart [37]. The impulse is discharged prematurely by an irritable focus in the atria giving rise to a distorted P wave, usually superimposed on the preceding T wave. As shown in Figure 9j, the proposed algorithms detected the merged T waves in PACs (record 209). As illustrated in Figure 9, the proposed method successfully detected T waves in ECG signals with a low SNR, baseline wander, and various arrhythmias. The performance of the

T wave detection algorithms is evaluated using two statistical measures: $\mathrm{SE} = \mathrm{TP}/(\mathrm{TP} + \mathrm{FN})$ and $+\mathrm{P} = \mathrm{TP}/(\mathrm{TP} + \mathrm{FP})$, where TP is the number of true positives (T wave peak detected within the range of 30 ms of the annotated T wave peak), FN is the number of false negatives (annotated T wave peak has not been detected), and FP is the number of false positives (T wave peak detected outside the range of 30 ms of the annotated T wave peak). The sensitivity SE reports the percentage of true beats that were correctly detected by the algorithm. The positive predictivity $+\mathrm{P}$ reports the percentage of beat detections that were true beats.

The abnormal heart rhythms caused a large number of FNs compared to the FPs. Table 1 shows the result of T wave detection over 48 records of the MIT-BIH database. FNs are mainly caused by noise and PVC, as in record 219, and atrial fibrillation, as in record 202. The algorithm achieved a sensitivity of 99.86% and a positive predictivity of 99.65%, which are promising results for handling the non-stationary effects, low SNR, PACs, PVCs, LBBBs, and RBBBs in ECG signals.

3.1. Comparison of Performance on the QT Database

The detection performance on the QT database obtained by the proposed T wave detector record by record performance is shown in Tables 2 and 3. The overall comparison of our results with the existing T wave detection algorithms on the QT database is demonstrated in Table 4. It summarizes the performances in terms of number of beats, methodology, SE, and +P. Note that the proposed algorithm scored slightly higher overall performances (average of SE and +P) than Martínez *et al.* [38] and Laguna *et al.* [39] over the manually annotated T waves. It is clear that the proposed algorithm succeeds in handling long ECG recordings with high performance over the 111,201 automatically annotated heart beats. Moreover, the proposed T wave detector has not been re-tuned over any databases, thus the results are promising, and the algorithm can detect T peaks over different databases, sampling frequencies, types of arrhythmias, and noise.

3.2. Processing Time

Less computational time is achieved when the simplest method is used (*i.e.*, the algorithm presented in this paper requires less computational time). This is advantageous in terms of future development of wearable and portable diagnostic devices, and in terms of helping online and real-time diagnoses.

It is misleading to suggest that mentioning the average speed of the proposed detector, over a certain time length of ECG signal, would provide a comparative result. This is because the processing time depends on the number of beats within each ECG recording, not on the record length. In this study, the T wave detector was implemented in MATLAB 2010b (The MathWorks, Inc., Natick, MA, USA) on Intel™ i5 CPU 2.27 GHz.

It is worth noting that the number of beats of the 15-min recordings category in QT database was relatively consistent—with a mean $\pm$ SD, number of beats 1059 ± 275—over all records of this category. On the contrary, the 30-min beat average, in MIT-BIH database, was 2291 with an SD of 448 beats. As the processing time depends on the number of beats rather than the recording length [25], we found, for example, the proposed detector took 2.58 s to process record 215-MITDB contains 3362 beats, while it took 0.28 s to process 527 beats in record 33-QTDB. In general, without taking the number of beats

into consideration, the speed of the proposed detector is fast. The suggested detector handles 15-min recordings in 0.52 ± 0.14 s, while it takes 1.98 ± 0.32 s to handle 30-min ECG recordings.

Table 1. T wave peak detection performance over the annotated MIT-BIH Arrhythmia database [20,21]. To evaluate the performance of the T wave detection algorithm, two statistical measures are used: $\mathrm{SE} = \mathrm{TP}/(\mathrm{TP} + \mathrm{FN})$ and $+\mathrm{P} = \mathrm{TP}/(\mathrm{TP} + \mathrm{FP})$, where TP is the number of true positives (T wave peak detected within the range of 30 ms of the annotated T wave peak), FN is the number of false negatives (annotated T wave peak has not been detected), and FP is the number of false positives (T wave peak detected outside the range of 30 ms of the annotated T wave peak).

Record	No of beats	TP	FP	FN	SE (%)	+P (%)
100	2274	2272	0	0	100.00	100.00
101	1866	1863	1	4	99.79	99.95
102	2187	2185	0	0	100.00	100.00
103	2084	2082	0	4	99.81	100.00
104	2229	2227	0	1	99.96	100.00
105	2602	2586	0	2	99.92	100.00
106	2026	2024	0	56	97.23	100.00
107	2136	2134	0	3	99.86	100.00
108	1763	1757	0	13	99.26	100.00
109	2533	2530	0	0	100.00	100.00
111	2123	2121	0	16	99.25	100.00
112	2539	2537	0	0	100.00	100.00
113	1794	1792	0	0	100.00	100.00
114	1890	1885	0	69	96.34	100.00
115	1953	1951	0	19	99.03	100.00
116	2395	2392	0	2	99.92	100.00
117	1535	1533	0	0	100.00	100.00
118	2278	2276	0	4	99.82	100.00
119	1988	1986	0	4	99.80	100.00
121	1863	1860	0	46	97.53	100.00
122	2476	2474	0	0	100.00	100.00
123	1519	1517	0	0	100.00	100.00
124	1619	1617	0	7	99.57	100.00
200	2601	2599	0	9	99.65	100.00
201	1949	1947	0	57	97.07	100.00
202	2138	2134	0	113	94.70	100.00
203	2988	2965	0	1	99.97	100.00
205	2656	2556	0	0	100.00	100.00
207	2324	2139	0	9	99.58	100.00
208	2953	2949	0	0	100.00	100.00
209	3006	3003	0	5	99.83	100.00
210	2652	2637	0	0	100.00	100.00
212	2748	2746	0	0	100.00	100.00
213	3250	3247	0	0	100.00	100.00
214	2262	2184	0	0	100.00	100.00
215	3362	3354	0	0	100.00	100.00
217	2208	2205	0	3	99.86	100.00
219	2154	2152	0	144	93.31	100.00
220	2048	2046	0	2	99.90	100.00
221	2427	2424	0	0	100.00	100.00
222	2485	2472	0	33	98.67	100.00
223	2604	2601	0	1	99.96	100.00
228	2060	2056	0	52	97.47	100.00
230	2256	2254	0	39	98.27	100.00
231	1571	1569	0	0	100.00	100.00
232	1783	1781	0	1	99.94	100.00
233	3077	2914	0	1	99.97	100.00
234	2751	2749	0	0	100.00	100.00
	109985	109284	1	720	99.28	100.00

Table 2. T wave peak detection performance over the manually annotated 11 recordings of the QT database [24]. To evaluate the performance of the T wave detection algorithm, two statistical measures are used: $\mathrm{SE} = \mathrm{TP}/(\mathrm{TP} + \mathrm{FN})$ and $+\mathrm{P} = \mathrm{TP}/(\mathrm{TP} + \mathrm{FP})$, where TP is the number of true positives (T wave peak detected within the range of 30 ms of the annotated T wave peak), FN is the number of false negatives (annotated T wave peak has not been detected), and FP is the number of false positives (T wave peak detected outside the range of 30 ms of the annotated T wave peak).

Record	No of beats	TP	FP	FN	SE (%)	+P (%)
sel100	30	30	0	0	100.00	100.00
sel102	85	85	0	0	100.00	100.00
sel103	30	30	0	0	100.00	100.00
sel104	77	75	0	0	100.00	100.00
sel114	50	50	0	0	100.00	100.00
sel116	50	49	0	0	100.00	100.00
sel117	30	30	0	0	100.00	100.00
sel123	30	30	0	0	100.00	100.00
sel213	71	71	0	0	100.00	100.00
sel221	30	29	1	1	96.67	96.67
sel223	31	31	0	0	100.00	100.00
sel230	50	42	9	8	84.00	82.35
sel231	50	50	0	0	100.00	100.00
sel232	30	30	0	0	100.00	100.00
sel233	30	30	0	0	100.00	100.00
sel301	30	30	0	0	100.00	100.00
sel302	30	30	0	0	100.00	100.00
sel306	36	32	0	0	100.00	100.00
sel307	30	30	0	0	100.00	100.00
sel308	50	40	10	10	80.00	80.00
sel310	30	30	0	0	100.00	100.00
sel803	30	30	4	0	100.00	88.24
sel808	30	30	0	0	100.00	100.00
sel811	30	30	0	0	100.00	100.00
sel820	30	30	0	0	100.00	100.00
sel821	30	30	0	0	100.00	100.00
sel840	70	70	0	0	100.00	100.00
sel847	33	33	0	0	100.00	100.00
sel853	30	30	0	0	100.00	100.00
sel871	70	70	0	0	100.00	100.00
sel872	30	30	0	0	100.00	100.00
sel873	33	33	0	0	100.00	100.00
sel883	30	30	0	0	100.00	100.00
sel891	71	71	0	0	100.00	100.00
sel16265	30	30	0	0	100.00	100.00
sel16272	30	30	0	0	100.00	100.00
sel16273	30	30	0	0	100.00	100.00
sel16420	30	30	0	0	100.00	100.00
sel16483	30	30	0	0	100.00	100.00
sel16539	30	30	0	0	100.00	100.00
sel16773	30	21	9	9	70.00	70.00
sel16786	30	30	0	0	100.00	100.00
sel16795	30	30	0	0	100.00	100.00
sel17453	30	30	0	0	100.00	100.00
sele0104	30	30	0	0	100.00	100.00
sele0106	30	30	0	0	100.00	100.00
sele0107	34	34	0	0	100.00	100.00
sele0110	30	30	0	0	100.00	100.00
sele0111	30	30	0	0	100.00	100.00
sele0112	50	50	0	0	100.00	100.00
sele0114	30	30	0	0	100.00	100.00
sele0116	30	30	0	0	100.00	100.00
sele0121	30	30	0	0	100.00	100.00
sele0122	30	30	0	0	100.00	100.00
sele0124	50	50	0	0	100.00	100.00
sele0126	30	25	4	5	83.33	86.21
sele0129	30	30	0	0	100.00	100.00
sele0133	30	30	0	0	100.00	100.00
sele0136	30	30	0	0	100.00	100.00
sele0166	36	36	0	0	100.00	100.00
sele0170	30	30	0	0	100.00	100.00
sele0203	30	30	0	0	100.00	100.00
sele0210	30	30	0	0	100.00	100.00
sele0211	30	30	0	0	100.00	100.00
sele0303	30	30	0	0	100.00	100.00
sele0405	30	30	0	0	100.00	100.00
sele0406	31	31	0	0	100.00	100.00
sele0409	30	30	0	0	100.00	100.00
sele0411	30	30	0	0	100.00	100.00
sele0509	30	30	0	0	100.00	100.00
sele0603	30	30	0	0	100.00	100.00
sele0604	30	30	0	0	100.00	100.00
sele0606	30	30	0	0	100.00	100.00
sele0607	30	30	0	0	100.00	100.00
sele0609	30	30	0	0	100.00	100.00
sele0612	30	30	0	0	100.00	100.00
sele0704	30	30	0	0	100.00	100.00
sel30	30	30	0	0	100.00	100.00
sel31	30	26	4	4	86.67	86.67
sel32	30	30	0	0	100.00	100.00
sel33	30	30	0	0	100.00	100.00
sel34	30	30	0	0	100.00	100.00
sel36	31	30	1	1	96.77	96.77
sel38	30	30	0	0	100.00	100.00
sel40	30	30	1	0	100.00	96.77
sel41	30	30	0	0	100.00	100.00
sel42	30	30	0	0	100.00	100.00
sel43	30	28	0	0	100.00	100.00
sel44	30	30	0	0	100.00	100.00
sel45	30	29	1	1	96.67	96.67
sel46	30	30	0	0	100.00	100.00
sel47	30	27	2	2	93.10	93.10
sel48	30	30	0	0	100.00	100.00
sel49	30	30	0	0	100.00	100.00
sel50	30	30	0	0	100.00	100.00
sel51	32	32	0	0	100.00	100.00
sel51	30	30	0	0	100.00	100.00
sel52	30	30	0	0	100.00	100.00
sel17152	30	30	0	0	100.00	100.00
sel14046	31	31	0	0	100.00	100.00
sel14157	30	30	0	0	100.00	100.00
sel14172	50	50	0	0	100.00	100.00
sel15814	30	30	0	0	100.00	100.00
	3542	3491	46	41	98.90	98.77

Table 3. T wave peak detection performance over the automatically annotated QT database [24]. To evaluate the performance of the T wave detection algorithm, two statistical measures are used: $\mathrm{SE} = \mathrm{TP}/(\mathrm{TP} + \mathrm{FN})$ and $+\mathrm{P} = \mathrm{TP}/(\mathrm{TP} + \mathrm{FP})$, where TP is the number of true positives (T wave peak detected within the range of 30 ms of the annotated T wave peak), FN is the number of false negatives (annotated T wave peak has not been detected), and FP is the number of false positives (T wave peak detected outside the range of 30 ms of the annotated T wave peak).

Record	No of beats	TP	FP	FN	SE (%)	+P (%)
sel100	1134	1132	0	1	99.91	100.00
sel102	1088	1086	0	2	99.82	100.00
sel103	1048	1046	4	5	99.52	99.62
sel104	1109	1107	9	10	99.10	99.19
sel114	867	864	1	7	99.19	99.88
sel116	1186	1184	0	25	97.89	100.00
sel117	766	764	0	1	99.87	100.00
sel123	756	754	0	0	100.00	100.00
sel213	1641	1639	1	2	99.88	99.94
sel221	1247	1244	0	116	90.68	100.00
sel223	1309	1307	0	6	99.54	100.00
sel230	1077	1075	115	200	81.41	88.40
sel231	732	730	0	1	99.86	100.00
sel232	866	864	18	19	97.80	97.92
sel233	1532	1265	13	112	91.79	98.97
sel301	1352	1348	0	0	100.00	100.00
sel302	1501	1498	1	2	99.87	99.93
sel306	1040	1038	0	30	97.11	100.00
sel307	853	851	0	1	99.88	100.00
sel308	1294	1292	19	21	98.38	98.53
sel310	2012	2008	0	3	99.85	100.00
sel803	1026	1024	0	84	91.80	100.00
sel808	903	901	24	29	96.78	97.32
sel811	704	702	0	1	99.86	100.00
sel820	1159	1157	1	3	99.74	99.91
sel821	1557	1555	2	3	99.81	99.87
sel840	1180	1178	1	2	99.83	99.92
sel847	803	799	0	3	99.62	100.00
sel853	1113	1110	6	8	99.28	99.46
sel871	917	915	2	3	99.67	99.78
sel872	990	988	0	2	99.80	100.00
sel873	859	857	0	1	99.88	100.00
sel883	892	890	30	36	95.96	96.61
sel891	1267	1265	0	1	99.92	100.00
sel16265	1031	1029	10	11	98.93	99.03
sel16272	851	849	0	1	99.88	100.00
sel16273	1112	1110	4	5	99.55	99.64
sel16420	1063	1061	0	1	99.91	100.00
sel16483	1087	1085	1	2	99.82	99.91
sel16539	922	920	0	1	99.89	100.00
sel16773	1008	1006	168	328	67.43	80.17
sel16786	925	923	0	1	99.89	100.00
sel16795	761	759	0	1	99.87	100.00
sel17453	1047	1045	0	1	99.90	100.00
sele0104	804	802	0	1	99.88	100.00
sele0106	897	894	0	1	99.89	100.00
sele0107	823	810	25	34	95.81	96.88
sele0110	872	870	1	3	99.66	99.88
sele0111	908	906	1	1	99.89	99.89
sele0112	684	682	121	189	72.33	80.33
sele0114	698	696	23	28	95.98	96.68
sele0116	560	557	1	3	99.46	99.82
sele0121	1434	1432	2	2	99.86	99.86
sele0122	1414	1412	0	1	99.93	100.00
sele0124	1121	1119	4	5	99.55	99.64
sele0126	945	943	83	793	16.00	64.53
sele0129	672	670	40	55	91.80	93.90
sele0133	840	838	0	1	99.88	100.00
sele0136	810	808	3	4	99.51	99.63
sele0166	813	811	0	1	99.88	100.00
sele0170	897	895	0	1	99.89	100.00
sele0203	1246	1244	0	4	99.68	100.00
sele0210	1063	1061	0	1	99.91	100.00
sele0211	1575	1573	0	1	99.94	100.00
sele0303	1045	1043	1	2	99.81	99.90
sele0405	1216	1214	0	57	95.30	100.00
sele0406	959	957	0	1	99.90	100.00
sele0409	1737	1735	0	1	99.94	100.00
sele0411	1202	1200	0	2	99.83	100.00
sele0509	1028	1026	0	39	96.20	100.00
sele0603	869	867	30	84	90.33	96.32
sele0604	1031	1029	0	2	99.81	100.00
sele0606	1442	1440	0	4	99.72	100.00
sele0607	1184	1182	0	0	100.00	100.00
sele0609	1127	1125	3	4	99.64	99.73
sele0612	751	749	0	1	99.87	100.00
sele0704	1094	1092	0	214	80.40	100.00
sel30	1018	1014	0	3	99.70	100.00
sel31	1087	1084	45	385	64.52	93.96
sel32	1196	1194	0	3	99.75	100.00
sel33	527	525	0	4	99.24	100.00
sel34	897	895	0	0	100.00	100.00
sel35	882	880	0	384	56.36	100.00
sel36	948	946	135	227	76.03	84.21
sel37	682	679	0	511	24.74	100.00
sel38	1563	1561	0	0	100.00	100.00
sel40	1171	1169	0	9	99.23	100.00
sel41	1069	1067	0	24	97.75	100.00
sel42	1366	1363	2	24	98.24	99.85
sel43	1247	1245	0	63	94.94	100.00
sel44	1430	1427	0	46	96.78	100.00
sel45	1337	1335	0	57	95.73	100.00
sel46	971	968	66	96	90.09	92.97
sel47	856	854	0	98	88.52	100.00
sel48	886	884	0	88	90.05	100.00
sel49	1398	1396	0	4	99.71	100.00
sel50	833	831	0	4	99.52	100.00
sel51	661	659	0	32	95.14	100.00
sel51	749	747	0	29	96.12	100.00
sel52	1411	1409	0	1	99.93	100.00
sel17152	1628	1626	0	0	100.00	100.00
sel14046	1260	1258	0	0	100.00	100.00
sel14157	1081	1079	0	9	99.17	100.00
sel14172	663	661	0	73	88.96	100.00
sel15814	1036	1034	0	34	96.71	100.00
	111201	110696	1016	4840	95.00	98.59

Table 4. T waves detection performance comparison on the QT database [24]. (N/R: not reported).

Publication	Method	# Beats	Annotation (File Name)	SE	+P
This work	Blocks of interest	111,201	Automatic (.pu)	95.0	98.59
This work	Blocks of interest	3542	Manual (.q1c)	98.90	98.77
Martinez *et al.* [38]	Wavelet	3542	Manual (.q1c)	99.77	97.79
Laguna *et al.* [39]	Low-pass-differentiator	3542	Manual (.q1c)	99.0	97.74
Vila *et al.* [40]	Modelling	3542	Manual (.q1c)	96.2	N/R

4. Limitations of Study and Future Work

The preliminary results are promising, especially after testing the algorithm on the QT database; however, testing the algorithm on a larger sample size is necessary to generalize the findings. In addition, a more focused study is needed to investigate atrial fibrillation, atrial flutter, paroxysmal supraventricular tachycardia, junctional tachycardia, and multifocal atrial tachycardia as the morphology of T waves may differ.

The presented method assumes that the R peaks are correctly detected. There is a linear correlation between the detection of T waves and the detected R peaks. If the R peaks are misclassified, this method will fail as it depends on the position of R peaks. However, this study provides a positive proof of concept for detecting T waves in arrhythmic ECG beats.

We created a rule-based system based on the three RR interval window proposed in [32]. Perhaps, it is important to investigate the development of a rule-based system based on more than three RR intervals to examine if it will improve the overall T wave detection accuracy. Moreover, the proposed method is based on several thresholds, which are calibrated using clinical knowledge. Clinical knowledge is considered the gold standard in our work; thus, the obtained thresholds were considered optimal. However, an open question for future work is to optimize all thresholds to improve accuracy.

One of the next steps regarding the results of this study is to detect arrhythmic ECG beats using the RT or ST interval as a main feature. In addition, the detection of P waves based on the accurate detection of T wave peaks needs to be examined. Moreover, perhaps, an optimization over the clinical parameters after splitting the databases into a training set and test set may improve the detection rate of the T waves. There is also a need to investigate the T-waves with different morphology, e.g., biphasic T-waves.

Technically, exploring the event-related moving average methodology for detecting events in ECG signals is promising in terms of computational complexity and efficiency. This can be further improved by investigating other bandpass filters with different orders and also by developing fast-moving average (or median) techniques for real-time analysis and mobile phone applications.

5. Conclusions

There is a limitation when evaluating T wave detection algorithms as datasets with annotated T waves are lacking. Consequently, comparing existing algorithms becomes even more difficult. Therefore, annotation of T waves is discussed and provided. Using these approaches, it is possible to support

diagnostic analysis, delivering important information for (differential) diagnosis to medical experts. Using mobile technologies with automatic analysis software driven by medical expert knowledge, it will be furthermore possible to provide screening and monitoring solutions in places where medical expertise is scarce, such as remote rural areas and developing countries.

The use of two moving averages is simple and computationally efficient for mobile electronic health tools, such as cell phones and telemedicine technologies. The assessment of the T detector has been reliably carried out over the existing standard databases (QT and MIT-BIH), which contain different beat types and morphologies found in ECG signals. The developed algorithm was evaluated on all ECG recordings in the MIT-BIH database, 48 self-annotated records containing a total of 109,985 heart beats. It achieved a sensitivity of 95% and a positive predictivity of 98.59% over the MIT-BIH ECG signals, which contain low SNR, baseline wander, paced beats, and various arrhythmias. Interestingly, the proposed algorithm succeeded in scoring the highest overall accuracy of 98.84% over the manually annotated QT database (3542 heart beats) when compared to the other three algorithms (*cf.* Table 4). Moreover, the algorithm scored a high overall accuracy of 96.7% over the automaticlly annotated QT database (111,201 heart beats). Overall, simplicity and efficiency are required in developing T wave detection algorithms for processing long-term recordings and large databases as well as for expanding our telemedicine capabilities in the near future.

Acknowledgments

Mohamed Elgendi gratefully acknowledges the Australian government and Charles Darwin University whose generous scholarships towards his PhD set the foundation for this research. He appreciates the support of Friso De Boer and acknowledges Gari Clifford for helpful discussions.

Author Contributions

ME designed the experiment. ME, BE, and DA performed the statistical analysis. ME, BE, and DA conceived of the study and drafted the manuscript. The authors approved the final manuscript.

Conflicts of Interest

The authors declare no conflict of interest.

References

1. Alwan, A. *Global Status Report on Noncommunicable Diseases 2010*; World Health Organization: Geneva, Switzerland, 2011.
2. Dilaveris, P.E.; Gialafos, E.J.; Sideris, S.K.; Theopistou, A.M.; Andrikopoulos, G.K.; Kyriakidis, M.; Gialafos, J.E.; Toutouzas, P.K. Simple electrocardiographic markers for the prediction of paroxysmal idiopathic atrial fibrillation. *Am. Heart J.* **1998**, *135*, 733–738.
3. Tsipouras, M.G.; Fotiadis, D.I.; Sideris, D. Arrhythmia classification using the RR-interval duration signal. In Proceedings of 2002 Computers in Cardiology, 22–25 September 2002; pp. 485–488.

4. Tran, T.; McNames, J.; Aboy, M.; Goldstein, B. Prediction of paroxysmal atrial fibrillation by analysis of atrial premature complexes. *IEEE Trans. Biomed. Eng.* **2004**, *51*, 561–569.
5. De Chazal, P.; O'Dwyer, M.; Reilly, R.B. Automatic classification of heartbeats using ECG morphology and heartbeat interval features. *IEEE Trans. Biomed. Eng.* **2004**, *51*, 1196–1206.
6. Krasteva, V.T.; Jekova, I.I.; Christov, I.I. Automatic detection of premature atrial contractions in the electrocardiogram. *Electrotech. Electron. E+E* **2006**, *9–10*, 49–55.
7. Scholz, U.J.; Bianchi, A.M.; Cerutti, S.; Kubicki, S. Vegetative background of sleep: Spectral analysis of the heart rate variability. *Physiol. Behav.* **1997**, *62*, 1037–1043.
8. Trinder, J.; Kleiman, J.; Carrington, M.; Smith, S.; Breen, S.; Tan, N.; Kim, Y. Autonomic activity during human sleep as a function of time and sleep stage. *J. Sleep Res.* **2001**, *10*, 253–264.
9. Zapanta, L.; Poon, C.; White, D.; Marcus, C.; Katz, E. Heart rate chaos in obstructive sleep apnea in children. In Proceedings of the 26th Annual International Conference of the IEEE Engineering in Medicine and Biology Society (IEMBS'04), San Francisco, CA, USA, 1–5 September 2004; pp. 3889–3892.
10. Shouldice, R.; O'Brien, L.; O'Brien, C.; de Chazal, P.; Gozal, D.; Heneghan, C. Detection of obstructive sleep apnea in pediatric subjects using surface lead electrocardiogram features. *Sleep* **2004**, *27*, 784–792.
11. Elgendi, M.; Eskofier, B.; Dokos, S.; Abbott, D. Revisiting QRS Detection Methodologies for Portable, Wearable, Battery-Operated, and Wireless ECG Systems. *PLoS ONE* **2014**, *9*, e84018.
12. Goutas, A.; Ferdi, Y.; Herbeuval, J.P.; Boudraa, M.; Boucheham, B. Digital fractional order differentiation-based algorithm for P and T-waves detection and delineation. *ITBM-RBM* **2005**, *26*, 127–132.
13. Wan, X.; Xu, D. An ECG T waves detection scheme based on the compensatory criterion. In Proceedings of the 2010 3rd International Conference on Biomedical Engineering and Informatics (BMEI), Yantai, China, 16–18 October 2010; Volume 2, pp. 730–734.
14. Vazquez-Seisdedos, C.; Neto, J.; Maranon Reyes, E.; Klautau, A.; de Oliveira, R.C.L. New approach for T-wave end detection on electrocardiogram: Performance in noisy conditions. *Biomed. Eng. Online* **2011**, *10*, doi:10.1186/1475-925X-10-77.
15. Nair, A.; Marziliano, P. P and T wave detectionon multichannel ECG using FRI. In Proceedings of the 2014 36th Annual International Conference of the IEEE Engineering in Medicine and Biology Society (EMBC), Chicago, IL, USA, 26–30 August 2014; pp. 2269–2273.
16. Clifford, G.D.; Azuaje, F.; McSharry, P. *Advanced Methods and Tools for ECG Data Analysis*; Artech House, Inc.: Norwood, MA, USA, 2006.
17. Hayden, G.; Brady, W.; Perron, A.; Somers, M.; Mattu, A. Electrocardiographic T-wave inversion: Differential diagnosis in the chest pain patient. *Am. J. Emerg. Med.* **2002**, *20*, 252–262.
18. Michael, S.; Brady, W.; Perron, A.; Mattu, A. The prominent T wave: Electrocardiographic differential diagnosis. *Am. J. Emerg. Med.* **2002**, *20*, 243–251.
19. Smith, D.; Nowacki, D.; Li, J.J. ECG T-Wave Monitor for Potential Early Detection and Diagnosis of Cardiac Arrhythmias. *Cardiovasc. Eng.* **2010**, *10*, 201–206.
20. Moody, G.B.; Mark, R.G. The impact of the MIT-BIH Arrhythmia Database. *IEEE Eng. Med. Biol. Mag.* **2001**, *20*, 45–50.

21. Goldberger, A.L.; Amaral, L.A.N.; Glass, L.; Hausdorff, J.M.; Ivanov, P.C.; Mark, R.G.; Mietus, J.E.; Moody, G.B.; Peng, C.K.; Stanley, H.E.; *et al.* PhysioBank, PhysioToolkit, and PhysioNet: Components of a New Research Resource for Complex Physiologic Signals. *Circulation* **2000**, *101*, e215–e220.
22. Willems, J.L.; Arnaud, P.; Bemmel, J.H.V.; Bourdillon, P.J.; Degani, R.; Denis, B.; Graham, I.; Harms, F.M.; Macfarlane, P.W.; Mazzocca, G.; *et al.* A reference data base for multilead electrocardiographic computer measurement programs. *J. Am. Coll. Cardiol.* **1987**, *10*, 1313–1321.
23. Elgendi, M. Annotation of P and T waves in MIT-BIH Arrhythmia Database. Available online: http://www.elgendi.net/databases.htm (accessed on 20 July 2015).
24. Laguna, P.; Mark, R.G.; Goldberg, A.; Moody, G.B. A database for evaluation of algorithms for measurement of QT and other waveform intervals in the ECG. In Proceedings of the IEEE Computers in Cardiology, Lund, Sweden, 7–10 September 1997; pp. 673–676.
25. Elgendi, M. Fast QRS Detection with an Optimized Knowledge-Based Method: Evaluation on 11 Standard ECG Databases. *PLoS ONE* **2013**, *8*, e73557.
26. Elgendi, M.; Jonkman, M.; de Boer, F. Frequency Bands Effects on QRS Detection. In Proceedings of the 3rd International Conference on Bio-Inspired Systems and Signal Processing (BIOSIGNALS 2010), Valencia, Spain, 20–23 January 2010; pp. 428–431.
27. Elgendi, M.; Norton, I.; Brearley, M.; Abbott, D.; Schuurmans, D. Systolic Peak Detection in Acceleration Photoplethysmograms Measured from Emergency Responders in Tropical Conditions. *PLoS ONE* **2013**, *8*, e76585.
28. Elgendi, M.; Norton, I.; Brearley, M.; Abbott, D.; Schuurmans, D. Detection of a and b waves in the acceleration photoplethysmogram. *Biomed. Eng. Online* **2014**, *13*, doi:10.1186/1475-925X-13-139.
29. Elgendi, M. Detection of c, d, and e waves in the acceleration photoplethysmogram. *Comput. Methods Programs Biomed.* **2014**, *117*, 125–136.
30. Thakor, N.V.; Webster, J.G.; Tompkins, W.J. Optimal QRS detector. *Med. Biol. Eng.* **1983**, *21*, 343–350.
31. Sahambi, J.S.; Tandon, S.N.; Bhatt, R.K.P. Using wavelet transforms for ECG characterization: An on-line digital signal processing system. *IEEE Eng. Med. Biol. Mag.* **1997**, *16*, 77–83.
32. Roskamm, H.; Csapo, G. *Disorders of Cardiac Function*, 1st ed.; Dekker: New York, NY, USA, 1982.
33. Elgendi, M.; Jonkman, M.; de Boer, F. Recognition of T waves in ECG signals. In Proceedings of the IEEE 35th Annual Northeast Bioengineering Conference, Boston, MA, USA, 3–5 April 2009; pp. 1–2.
34. Trahanias, P. An approach to QRS complex detection using mathematical morphology. *IEEE Trans. Biomed. Eng.* **1993**, *40*, 201–205.
35. Laguna, P.; Thakor, N.; Caminal, P.; Jané, R.; Yoon, H.R.; de Luna, A.B.; Marti, V.; Guindo, J. New algorithm for QT interval analysis in 24-h Holter ECG: Performance and applications. *Med. Biol. Eng. Comput.* **1990**, *28*, 67–73.

36. Schimpf, R.; Wolpert, C.; Bianchi, F.; Giustetto, C.; Gaita, F.; Bauersfeld, U.; Borggrefe, M. Congenital short QT syndrome and implantable cardioverter defibrillator treatment: Inherent risk for inappropriate shock delivery. *J. Cardiovasc. Electrophysiol.* **2003**, *14*, 1273–1277.
37. Braunwald, E.; Zipes, D.; Libby, P.; Bonow, R. *Braunwald's Heart Disease: A Textbook of Cardiovascular Medicine*, 7th ed.; Saunders: Philadelphia, PA, USA, 2004.
38. Martínez, J.P.; Almeida, R.; Olmos, S.; Rocha, A.P.; Laguna, P. A wavelet-based ECG delineator: Evaluation on standard databases. *IEEE Trans. Biomed. Eng.* **2004**, *51*, 570–581.
39. Laguna, P.; Jané, R.; Caminal, P. Automatic detection of wave boundaries in multilead ECG signals: Validation with the CSE database. *Comput. Biomed. Res.* **1994**, *27*, 45–60.
40. Vila, J.; Gang, Y.; Presedo, J.; Fernandez-Delgado, M.; Barro, S.; Malik, M. A new approach for TU complex characterization. *IEEE Trans. Biomed. Eng.* **2000**, *47*, 764–772.